
Article:
Schröter, Sandra orcid.org/0000-0003-1029-4041, Gibson, Andrew Robert orcid.org/0000-0002-1082-4359, Kushner, M . J. et al. (2 more authors) (2018) Numerical study of the influence of surface reaction probabilities on reactive species in an rf atmospheric pressure plasma containing humidity. Plasma Physics and Controlled Fusion. pp. 1-10. ISSN 1361-6587

https://doi.org/10.1088/1361-6587/aa8fe9

Numerical study of the influence of surface reaction probabilities on reactive species in an rf atmospheric pressure plasma containing humidity

Sandra Schröter[1], Andrew R. Gibson[1,2], Mark J. Kushner[3], Timo Gans[1], Deborah O'Connell[1]

[1] York Plasma Institute, Department of Physics, University of York, Heslington, York YO10 5DD, United Kingdom

[2] LPP, CNRS, Ecole Polytechnique, UPMC Univ. Paris-Sud, Observatoire de Paris, Université Paris-Saclay, Sorbonne Universités, PSL Research University, 91128 Palaiseau, France

[3] University of Michigan, Department of Electrical Engineering and Computer Science, 1301 Beal Avenue, Ann Arbor, MI 48109-2122, USA

Abstract. The quantification and control of reactive species in atmospheric pressure plasmas is of great interest for their technological applications, in particular in biomedicine. Of key importance in simulating the densities of these species are fundamental data on their production and destruction. In particular, data concerning particle-surface reaction probabilities in atmospheric pressure plasmas are scarce, with most of these probabilities measured in low-pressure systems. In this work, the role of surface reaction probabilities, γ, of reactive neutral species (H, O and OH) on neutral particle densities in a He-H_2O rf atmospheric pressure microplasma jet (COST-µAPPJ) are investigated using a global model. It is found that the choice of γ, particularly for low-mass species having large diffusivities, such as H, can change computed species densities significantly. The importance of γ even at elevated pressures offers potential for tailoring the reactive species composition of atmospheric pressure microplasmas by choosing different wall materials or plasma geometries.

1. Introduction

Low-temperature atmospheric pressure plasmas (APPs) are sources of a range of biologically relevant reactive species (RS), making them suitable for biomedical applications [1–4], such as cancer treatment [5–9], wound healing [10, 11], or sterilisation [12, 13]. However, for the full potential of low-temperature plasmas to be realised in these applications, methods to predictably control the production and transport of RS are required. Numerical simulations are an important tool to understand RS production in APPs. In particular, global models [14–22] are often used to gain insight into the plasma-chemical kinetics of APPs, as they can incorporate large reaction

mechanisms taking into account tens of species and hundreds of reactions at low computational cost.

The results of such simulations, particularly species densities, are strongly dependent on the accuracy of fundamental chemical kinetics data. In this context, two types of reaction can be distinguished: those occurring in the gas-phase and those involving interactions with surfaces. For gas-phase chemical reactions, it has recently been shown [21], for a He-O_2 plasma, that varying the associated gas-phase rate coefficients within their stated uncertainties can lead to large variations in simulated species densities of importance for biomedical applications, such as O_3.

Surface interactions are known to be important production and loss channels of reactive species and energy in low-temperature plasmas produced at low pressure [23–26]. However, the role of surface interactions in APPs is less well known. It is often assumed that the rates of surface loss or production of species are significantly lower than those of gas-phase processes due to the low rate of diffusion of particles towards surfaces at high gas densities. Most numerical models of APPs take particle reactions at surfaces into account using surface reaction probabilities γ measured in low pressure systems. Surface reactions can generally be classified into the Langmuir-Hinshelwood (LH) mechanism or the Eley-Rideal (ER) mechanism. In the LH mechanism, gas phase species first adsorb onto the surface and reactions occur between two adsorbed species. In the ER mechanism, a gas phase species reacts with an adsorbed species. In both cases, the surface reaction rates depend on the surface coverage of reactants and the fluxes of species incident onto the surface. As a result, reaction probabilities are strongly dependent on experimental conditions, such as pressure and gas mixture [27–29], wall material [25, 26, 28, 30–34], temperature [35–37], and surface roughness [36, 37]. Ion bombardment can have a significant effect on the value of γ [27, 38] through the generation of free surface sites and desorption of adsorbates. If reactive gases are used in the system, plasma products can deposit on the chamber walls, and change γ over time [39], leading to drifts in the properties of the plasma [40].

Since γ depends on a number of different parameters it is important to carefully consider if values measured in one particular system can be reliably transferred to a second system with different operating conditions. Given that most measurements of surface reaction coefficients have been carried out at low pressures, their use to analyze experiments (or in simulations) at atmospheric pressure should consider the differences in operating conditions. The first step to achieve a greater understanding of the impact of surface reaction probabilities in APPs is to investigate their influence on species densities. In this work, a zero-dimensional plasma-chemical kinetics simulation (global model) is used to investigate the sensitivity of reactive species densities to the surface reaction probability of several important species in He-H_2O APPs.

The plasma investigated here is a radio-frequency (rf) atmospheric pressure plasma sustained in a He-H_2O feed gas, which is relevant for biomedical applications. This relevance stems from the ability to produce a range of biologically active RS such as O, H, OH, HO_2 and H_2O_2 [20, 41–45]. In addition, H_2O is typically present in the vicinity of

APPs if they are used in ambient air conditions, or as a liquid layer if biomedical samples are treated. As a result, understanding the chemical kinetics in plasmas containing H_2O is of significant interest. It is well known that H_2O rapidly adsorbs onto surfaces [46] and due to its polar nature, requires high temperatures (bake-out) to remove from the system. Since most APPs are operated without bake-out, it is likely that H_2O impurities are present even when using high purity gases. Therefore, values of γ may be subject to change depending on whether adsorbed water is present and in what quantities.

2. Description of Model

In this work, the zero-dimensional plasma-chemical kinetics simulation code GlobalKin [19] is used. GlobalKin solves the particle balance equation for neutral and charged particles eq. (1), and the energy balance equation for electrons eq. (2).

$$\frac{dN_i}{dt} = \frac{S}{V}\left(-\frac{D_i N_i \gamma_i}{\gamma_i \Lambda_D + \frac{4D_i}{v_{th,i}}} + \sum_j \frac{D_j N_j \gamma_j f_{ij}}{\gamma_j \Lambda_D + \frac{4D_j}{v_{th,j}}}\right) + S_i \tag{1}$$

$$\frac{d}{dt}\left(\frac{3}{2} n_e k_B T_e\right) = P_d - \sum_i \frac{3}{2} n_e \nu_{mi} \left(\frac{2m_e}{M_i}\right) k_B \left(T_e - T_i\right) + \sum_l n_e k_l N_l \Delta\epsilon_l \tag{2}$$

where N is the number density of particle i, Λ_D is the diffusion length, D is the diffusion coefficient and $v_{th,i}$ is the thermal velocity of species i. j denotes a species incident on the surface, which after a surface interaction returns to the gas phase as species i, γ the surface reaction coefficient, f the return fraction of species i after the surface reaction of species j. S_i is a source term which includes production and loss of species i through gas phase interactions. n_e is the number density of electrons, T_e the electron temperature, P_d the power input, m_e and M_i the electron and heavy particle masses, respectively, ν_{mi} the electron collision frequency, k_l represents gas-phase reaction rate coefficients, and $\Delta\epsilon_l$ the electron energy loss during inelastic collisions. In order to investigate the dominant reaction pathways for the formation and consumption of species, the pathway analysis tool PumpKin [47] is used.

The plasma source investigated is the COST reference micro-atmospheric pressure plasma jet (μAPPJ), as described by Golda *et al.* [48]. The μAPPJ consists of two plane-parallel stainless steel electrodes and two glass windows enclosing a $(3 \times 0.1 \times 0.1)$ cm^3 plasma channel. In this work, a power per unit volume of $P_d = 16.7$ Wcm^{-3} (corresponding to a power of 0.5 W in the standard COST μAPPJ geometry) and a constant gas temperature $T_g = 315$ K are assumed. The gas flow consists of 0.5 slm helium (He) with small admixtures of H_2O, which are 10 ppm and 5000 ppm, respectively. These correspond to typical experimental operating conditions. The smaller admixture of 10 ppm represents a typical water impurity content that may arise from the feed gas supply [49]. This may be considered as a typical un-intentional water impurity content. The higher admixture of 5000 ppm is in the typical order of an intentional water vapour admixture for the production of hydrogen and oxygen

Table 1: Species considered in the simulation.

Species	**neutral**	**positive**	**negative**
He	He, He^*, He_2^*	He^+, He_2^+	
O-species	O, $O(^1D)$, $O(^1S)$, O_2, $O_2(a^1\Delta)$, $O_2(b^1\Sigma)$, O_3	O^+, O_2^+, O_4^+	O^-, O_2^-
H-species	H, H_2		H^-
OH-species	OH, HO_2, H_2O, H_2O_2	OH^+, $H_2O^+(H_2O)_{n=0,1}$, $H^+(H_2O)_{n=1..9}$, $O_2^+(H_2O)$	OH^-, $H_2O_2^-$, $OH^-(H_2O)_{n=1..3}$
others			e

containing RS in this type of plasma [42, 44]. The surface area-to-volume ratio $\frac{S}{V}$ and the diffusion length Λ_D are

$$\frac{S}{V} = \frac{(4 \times 0.1 \times 3)\ \text{cm}^2}{(0.1 \times 0.1 \times 3)\ \text{cm}^3} = 40\ \text{cm}^{-1} \tag{3}$$

$$\Lambda_D = \left(\sqrt{2 \left(\frac{\pi}{0.1\ \text{cm}} \right)^2 + \left(\frac{\pi}{3\ \text{cm}} \right)^2} \right)^{-1} = 0.0225\ \text{cm} \tag{4}$$

Previous works have used variations of the μAPPJ by varying the gap distance and/or the electrode width, thereby changing the surface area-to-volume ratio and diffusion length and, potentially, the influence of surface processes [50–52]. To investigate the degree to which the plasma properties change in these systems simulations are also performed with varying electrode separation and electrode width.

The reaction mechanism takes into account 43 species, which are listed in table 1, and 386 bulk reactions, which can be found in reference [53]. The reaction mechanism is based on that described by Liu et al. [20], with some revised reaction rate coefficients.

For the "base case" simulation, surface reaction coefficients γ are generally assumed to be 0 for all neutral (γ_n) and negative ion species (γ_-), since negative ions are typically trapped in the positive plasma potential. For positive ions, $\gamma_+ = 1$, and it is assumed that they return as their neutral counter-part with a return fraction $f = 1$. For positive cluster ions (such as O_4^+, or $H^+(H_2O)_n$), the particles are assumed to return as basic fragments (two O_2 molecules or H and $n \times H_2O$). For electrons, the assumptions is $\gamma_e = 1$ and $f_{ej} = 0$ are used, implying that all electrons reaching the reactor surface take part in neutralizing reactions with positive ions (dielectric surfaces) or constitute current (metal surfaces).

In the following sections the role of surface reaction coefficients for H, O and OH are investigated with respect to the base case simulation. In the case of H and O, surface reactions are assumed to proceed via recombination to the equivalent molecules:

$$H \rightarrow \frac{1}{2} H_2 \tag{5}$$

$$O \rightarrow \frac{1}{2}O_2 \tag{6}$$

In the case of OH, the effect of assuming different surface reaction probabilities as well as two distinct return pathways are assessed:

$$OH \rightarrow \frac{1}{2}H_2O_2 \tag{7}$$

$$OH \rightarrow \frac{1}{2}(O + H_2O) \tag{8}$$

The role of these surface reactions in determining the plasma properties, including the percentage contribution of surface reactions to the total loss rate for each species, will be assessed for different values of γ, water admixture and electrode separation. These percentages are of course specific to the reaction rate coefficients used for gas-phase processes in this work as well as the specific plasma conditions. However, the trends presented as a function of each investigated parameter are thought to be relatively general.

3. Consequences of surface reactions in APPs

3.1. Role of γ_H and γ_O

The densities of neutral species and electrons as a function of γ for H (top) and O (bottom) at 10 ppm ((a) and (c)) and 5000 ppm ((b) and (d)) H_2O content are shown in fig. 1. The densities are normalised to the values obtained for the base case where $\gamma = 0$ for all neutral species. The neutral species and electron densities for the base case simulations at 10 and 5000 ppm H_2O content at the exit of the plasma channel are listed in tab. 2. γ is varied over a large range, from 0 to 1. This wide range reflects the lack of measurements of γ in APPs meaning that the precise range in which γ lies in these sources is difficult to specify *a priori*. The range over which γ is likely to vary as a result of changes in plasma parameters and/or surface material in APPs will be a subset of the total range considered in this investigation. As a result, the changes in species densities shown in this work represent the maximum possible range of variation for the given operating conditions.

Fig. 1 (a) and (b) show the evolution of normalised species densities under a variation of γ_H. It is assumed that H recombines at surfaces to form H_2. H is dominantly produced by electron impact dissociation of H_2O and decomposition of protonated water clusters through electron-ion recombination. At low H_2O content (fig. 1 (a)), when γ_H is increased from 0 to 1, the H density decreases to 0.12 of the base case simulation value due to the higher surfaces losses. For $\gamma_H = 1$, 99% of the loss of H is via surface recombination. The normalised H density reaches a minimum above $\gamma_H = 1 \times 10^{-2}$ when surface losses become limited by the ability of H to reach the surface due to diffusion (diffusion limited regime). H is relatively un-reactive in He/H_2O mixtures with trace amounts of H_2O. The reaction rate coefficient for H + H_2O has a high activation energy,

Table 2: Neutral species and electron densities at the exit of the plasma channel for the base case simulations at 10 and 5000 ppm H_2O content.

Species	**Density (cm^{-3}) - 10 ppm H_2O**	**Density (cm^{-3}) - 5000 ppm H_2O**
He^*	3.3×10^{10}	2.0×10^{9}
He_2^*	8.2×10^{9}	8.7×10^{5}
H	4.4×10^{13}	1.4×10^{15}
H_2	6.3×10^{11}	1.8×10^{15}
O	1.9×10^{12}	2.4×10^{13}
$O(^1D)$	5.6×10^{9}	3.2×10^{9}
O_2	2.2×10^{12}	7.8×10^{14}
$O_2(a^1\Delta)$	7.1×10^{10}	2.8×10^{13}
$O_2(b^1\Sigma)$	1.2×10^{10}	1.2×10^{10}
O_3	2.4×10^{7}	5.4×10^{9}
OH	2.7×10^{13}	4.5×10^{14}
HO_2	2.1×10^{10}	5.1×10^{12}
H_2O_2	2.5×10^{12}	5.9×10^{14}
e	9.9×10^{10}	4.6×10^{10}

and therefore has a negligible rate coefficient at ambient temperatures. As a result, H only reacts at significant rates with products produced in the plasma. Consequently, the majority of H produced in the gas-phase reaches the surface. Other species are directly affected by the drop in H densities with increasing γ. According to eq. 5, the H_2 density is strongly coupled to the H density, and increases by a factor 32 when γ_H is varied from 0 to 1. O_3, whose main consumption pathway is

$$H + O_3 \rightarrow OH + O_2 \tag{9}$$

increases by a factor 2.2 under the same variation due to the decrease in H density. However, it should be noted that O_3 densities are generally low in H_2O containing plasmas (see tab. 2), and O_3 is therefore a species with low relevance for the overall plasma chemistry.

HO_2 is another species whose density increases with increasing γ_H by a factor of about 1.5 over the whole range. H plays an important role in both the production and consumption of HO_2

$$H + O_2 + He \rightarrow HO_2 + He \tag{10}$$

$$H + HO_2 \rightarrow 2OH \tag{11}$$

Under the simulated conditions, these pathways contribute 18% and 46% to the production and loss of HO_2, respectively, when $\gamma_H = 0$. Their contributions decrease to 3% and 12%, respectively when $\gamma_H = 1$, due to the lower H density. As the relative

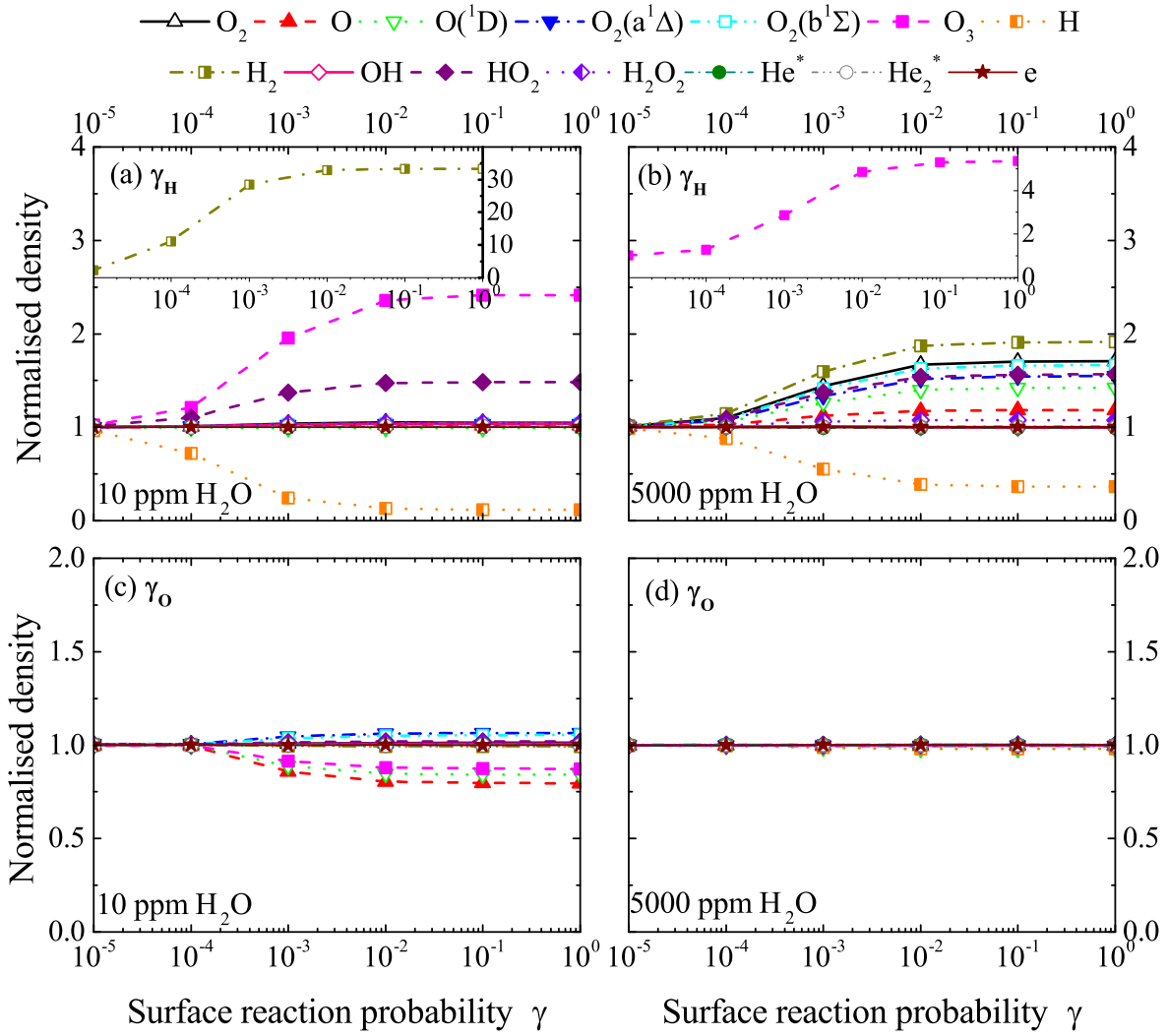

Figure 1: Species densities normalised to the base case simulation, where $\gamma = 0$ for all neutral species, as a function of surface loss coefficient for H ((a) and (b)) and O ((c) and (d)) for 10 ppm ((a) and (c)) and 5000 ppm ((b) and (d)) H_2O feed gas content. Insets show species with particularly large variations.

contribution of H to the destruction of HO_2 is larger than that for its production, the HO_2 density increases with increasing γ_H and lower H densities.

At high H_2O content (fig. 1 (b)), the main species influenced by a change of γ_H are H (decrease to 0.36 of the base case simulation value) O_3 (increase by a factor 5.4), and H_2 (increase by a factor 1.9). In general, the effect of the surface reaction coefficient on absolute species densities is decreased (with the exception of O_3), but more species are affected at 5000 ppm compared to 10 ppm H_2O. Species with relative density changes of more than 10% are O_2 (factor 1.7), O (1.2), $O(^1D)$ (1.4), $O_2(a^1\Delta)$ (1.6), and $O_2(b^1\Sigma)$ (1.7). The decreased importance of γ_H in determining the H density at high H_2O content is a result of the higher densities of species with which H can react in the gas phase compared to the low H_2O content case. As a result, the overall kinetics of H are less

affected by surface processes at high H_2O content. For $\gamma_H = 1$, 67% of the loss of H is via surface recombination, compared with 99% for the previously considered low water content of 10 ppm.

In general, the importance of H surface losses despite the high background gas pressure is a result of its large diffusion coefficient, which scales inversely with the mass of the particle, and its lack of exothermic reactions with feedstock gases. Heavier species, and those that have larger reaction rate coefficients with feedstock gases, are therefore less likely to be sensitive to wall reactions for a given plasma geometry. An example is atomic oxygen, whose sticking coefficient γ_O is varied in fig. 1 (c) and (d) for two different H_2O contents. Similarly to the previously studied case of H, it is assumed that O recombines at the wall to form O_2.

It is clear that the variation of γ_O (fig. 1 (c) and (d)) only results in small changes in species densities compared to the variation of γ_H. For $\gamma_O = 1$, 28% of the loss of O is via surface recombination for the low water content case. For the high water content case, surface recombination of O contributes only 2% to the total loss of O. Other species most affected by a change of γ_O are the purely oxygen containing species like O itself as well as $O(^1D)$ and O_3, all of which have comparably low densities in H_2O containing plasmas. However, the relative change does not exceed 20% under all investigated conditions and species. Under all simulated conditions, the consumption of O is dominated in the gas phase by collisions with OH, which, due to the relatively low diffusion coefficient of O, limits the importance of surface consumption pathways.

3.2. Role of γ_{OH} and return species

Another important assumption when considering surface reaction processes is the identity of the return species. A key species in H_2O containing plasmas is the hydroxyl radical (OH), which is produced mainly by electron impact dissociation of water and collisions between H_2O^+ and H_2O, where the H_2O^+ ion is produced via Penning ionisation of H_2O by excited states of He and He_2 [54]. Fig. 2 shows species densities as a function of γ_{OH}, under the assumption of different return species channels. The two return species channels investigated are given in eqs. 7 and 8, which are important consumption mechanisms for OH in the gas phase and consequently have the potential to occur as surface processes as well.

Fig. 2 (a) shows a variation of normalised species densities where OH surface reactions are assumed to proceed via eq. (7) at low feed gas H_2O content (10 ppm). Towards increasing γ_{OH}, absolute densities of OH decrease due to higher surface consumption with surface consumption becoming diffusion limited around $\gamma_{OH} = 1 \times 10^{-2}$. When $\gamma_{OH} = 1$, 52% of the total loss of OH is via surface recombination. As a direct result of eq. (7), H_2O_2 densities increase by over a factor of 2.6 between $\gamma_{OH} = 0$ and 1. With $\gamma_{OH} = 1$, surface recombination of OH is the main production mechanism (75%) for H_2O_2 under the investigated conditions. HO_2 also increases because the

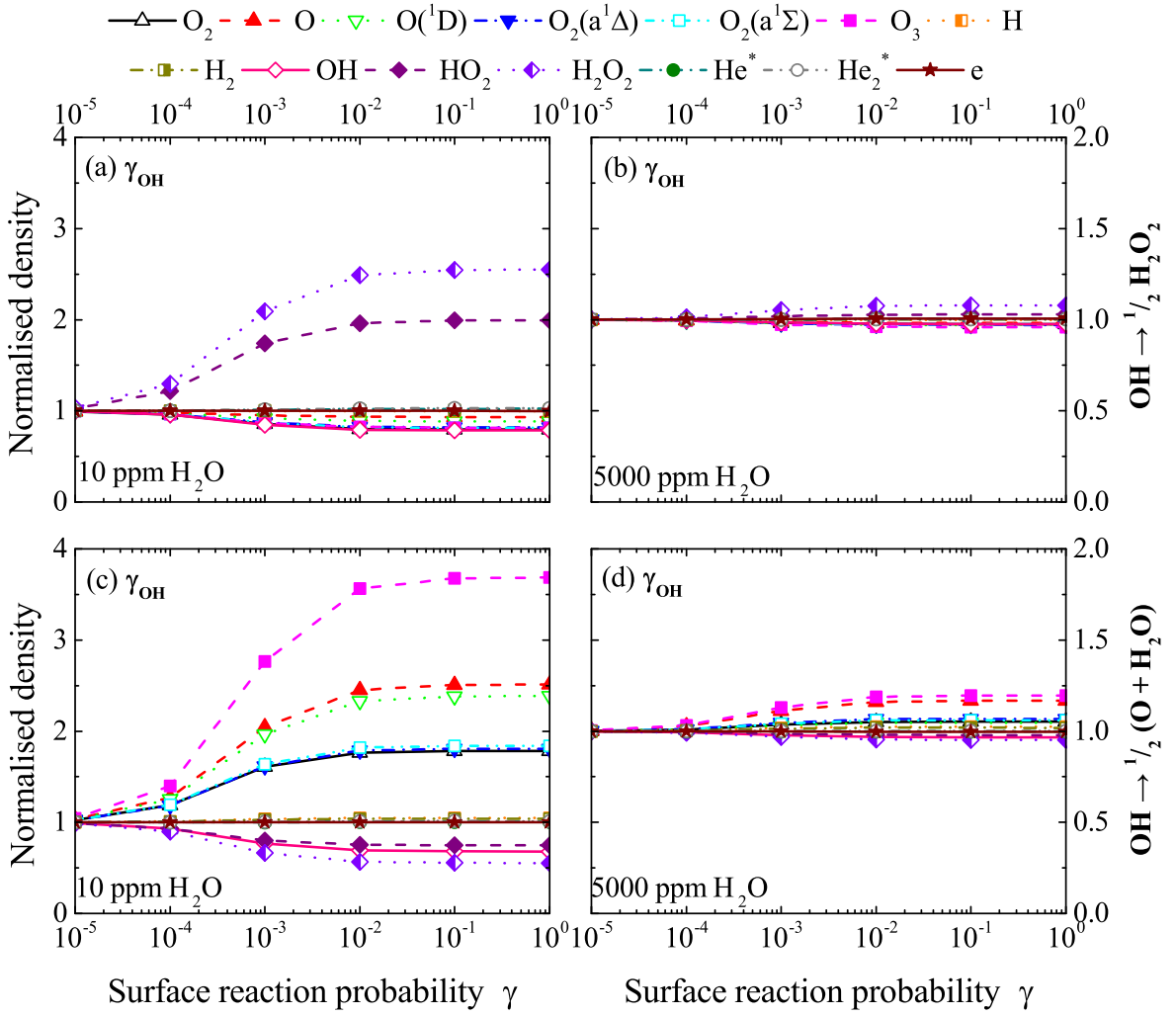

Figure 2: Normalised species densities as a function of γ_{OH}, where the return species are $\frac{1}{2}H_2O_2$ ((a) and (b)) and $\frac{1}{2}(O + H_2O)$ ((c) and (d)) for 10 ppm ((a) and (c)) and 5000 ppm ((b) and (d)) H_2O content.

density of OH decreases leading to reduced consumption of HO_2 via the reaction

$$HO_2 + OH \rightarrow H_2O + O_2 \tag{12}$$

In addition, a number of other species decrease with increasing γ_{OH} such as O_2 (21%), O_3 (19%), and $O_2(a^1\Delta)$ (18%), and to a lesser extent O (7%) and $O(^1D)$ (11%).

The decrease in O density is related to the decrease of the total rate for the reaction

$$2OH \rightarrow H_2O + O \tag{13}$$

The decrease of O_2 is directly caused by the decreasing O and OH densities and the reduced rate for the reaction

$$OH + O \rightarrow O_2 + H \tag{14}$$

which is the main production channel of O_2 at 10 ppm H_2O content under the investigated conditions. The atomic and molecular oxygen metastables are produced

directly from ground state O_2 and O via electron impact dissociation and excitation processes and therefore are strongly coupled to their densities. The production of O_3 relies strongly on the densities of O and O_2, and therefore also decreases towards higher γ_{OH}

$$O + O_2 + He \rightarrow O_3 + He \tag{15}$$

Assuming eq. (8) as the destruction pathway for OH at surfaces, species densities develop completely differently with γ_{OH} as shown in fig. 2 (c) for 10 ppm H_2O content. In this case, surface reactions account for 49% of the total loss of OH when $\gamma_{OH} = 1$. This is similar to the case for the previously discussed pathway where surface reactions of OH proceed via eq. (7). However, the trends for other species densities of interest are reversed compared with the case where surface reactions proceed via eq. (7), with purely oxygen containing species increasing (O_3 by a factor of 3.7, O factor 2.5, $O(^1D)$ factor 2.4, O_2 and its metastable states on average factor 1.8), while H_2O_2 and HO_2 are decreasing (45% and 25%, respectively).

The increase in the densities of O containing species can be explained by the enhanced production of O at surfaces at high γ_{OH}, according to eq. (8). At $\gamma_{OH} = 1$, 60% of the atomic oxygen is produced via eq. (8) at 10 ppm H_2O admixture. Atomic oxygen metastables also increase due to the previously discussed dependence on atomic oxygen. O_2, mainly created via eq. (14), increases less than atomic oxygen due to the decrease in the rate of eq. (14) as a result of the lower OH density, which offsets the increase in O.

The decrease of H_2O_2, at low H_2O content, with increasing γ_{OH} can be explained by the decreased OH density as H_2O_2 is mainly created via the reaction

$$2OH + He \rightarrow H_2O_2 + He \tag{16}$$

The decrease of HO_2 is directly related to the decrease of H_2O_2 via its main production pathway

$$OH + H_2O_2 \rightarrow HO_2 + H_2O \tag{17}$$

In the cases where the H_2O content is 5000 ppm (fig. 2 (b) and (d)), surface recombination has a much smaller effect on species densities, although some slight increases are still observed, with species developing similarly to the low H_2O admixture cases. However, in general, the plasma chemistry in these cases is dominated by gas-phase reactions with surface interactions playing a minor role in the overall reaction kinetics. In these cases, surface reactions account for only 4% of the total loss of OH. For the case where surface recombination proceeds via eq. (7), 17% of H_2O_2 is still produced at surfaces when $\gamma_{OH} = 1$ (compared to 75% in the low admixture case). For the case where surface recombination proceeds via eq. (8), 17% of O is produced at surfaces when $\gamma_{OH} = 1$, compared to 60% in the low admixture case.

Table 3: Neutral species densities at the exit of the plasma channel for $d = 0.05$ cm at 10 ppm and 5000 ppm H_2O content.

Species	**Density (cm^{-3}) - 10 ppm H_2O**	**Density (cm^{-3}) - 5000 ppm H_2O**
H	1.3×10^{12}	1.8×10^{14}
O	7.2×10^{11}	2.7×10^{13}
OH	1.5×10^{13}	3.9×10^{14}

3.3. Influence of reactor geometry

Overall, the relative importance of surface processes in determining the overall reactive species composition of the plasma is related to the competition between the rates of gas and surface phase processes. This is related to the surface-to-volume ratio and the diffusion length, which are defined by the reactor geometry. Surface processes are capable of influencing the reactive species chemistry when the dimensions of the COST μAPPJ is used in the model. Given the fact that μAPPJs can be produced using a variety of different dimensions, surface-to-volume ratios and diffusion lengths, it is also important to consider the role played by these parameters defining the reactive species composition of the plasma.

For this study, the assumptions $\gamma_+ = 1$ and $\gamma_- = 0$ are used, as previously. For electrons, a surface loss probability of $\gamma_e = 1$ is assumed. In addition, $\gamma_n = 0$, except for the previously discussed species H, O, and OH for which typical surface reaction probabilities measured in low pressure systems are assumed. These are $\gamma_H = 0.03$ [20, 55], $\gamma_O = 0.02$ [20, 32] and $\gamma_{OH} = 0.003$ [56]. However, it should be emphasized that these coefficients can significantly depend on plasma conditions, pressure, gas and wall temperatures, and wall materials, as discussed previously. The products of the recombination reactions are assumed as H_2, O_2, and H_2O_2, respectively, according to eqs. (5) to (7).

In order to investigate the role of the plasma dimensions, a square cross section of area $A = d^2$, is assumed. In analogy to the COST μAPPJ, d represents the inter-electrode distance and the electrode width. The inter-electrode distance is varied between $d = 0.05$ and 0.3 cm, which represents a typical range in which parallel plate APPs are operated. This corresponds to a variation in $\frac{S}{V}$ between 80 and 13.3 cm^{-1} and in Λ_D of $1.1{\times}10^{-2}$ and $6.7{\times}10^{-2}$ cm .

Fig. 3 shows densities of H, O and OH, normalised to their values at $d = 0.05$ cm (shown in tab. 3), as a function of inter-electrode distance for two different H_2O contents. The points depicted as stars correspond to the inter-electrode distance of the COST μAPPJ considered in the previous section. In the simulation, both the flow velocity and power per unit volume are kept constant at 916 and 966 cm/s (for 10 and 5000 ppm H_2O content, respectively) and 16.7 W/cm^3 so that the plasma conditions are comparable throughout the variation of d.

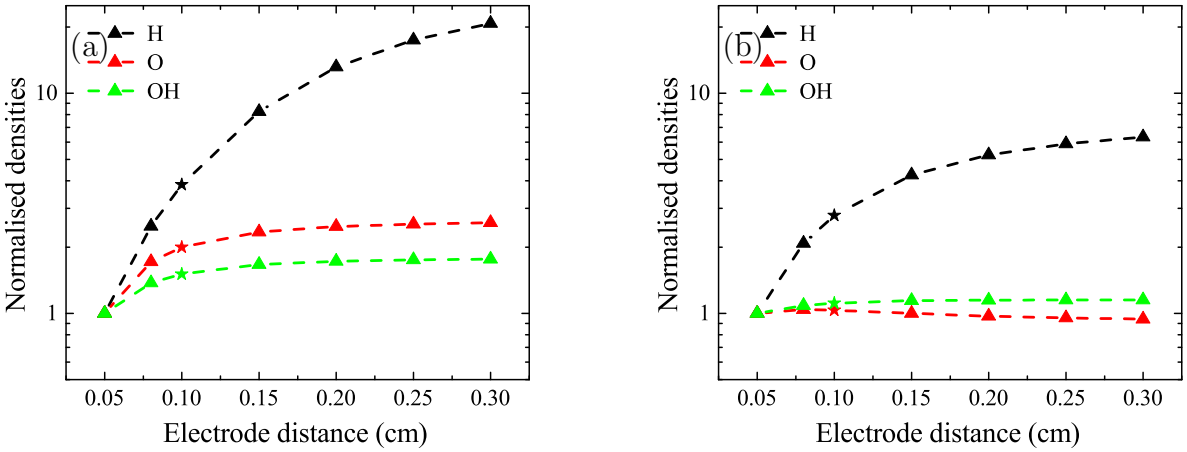

Figure 3: H, O, and OH densities, normalised to their values at $d = 0.05$ cm, as a function of inter-electrode distance for (a) 10 ppm and (b) 5000 ppm H_2O. The flow velocity is constant at 916 (a) and 966 cm/s (b). The power per unit volume is kept constant at 16.7 W/cm^3 for all points.

Examining fig. 3 (a), the densities of the three investigated species are shown to increase with increasing inter-electrode distance. The density of H, which has the highest diffusion coefficient of the investigated species, is particularly affected, increasing by more than an order of magnitude over the investigated range due to the decreased importance of surface losses as the diffusion length increases and the surface-to-volume ratio decreases. Towards the largest inter-electrode distances investigated, the density of H begins to approach a constant value indicating that the surface loss of H is beginning to be limited by its ability to reach the surface, through diffusion and competition from gas phase reactions. The higher mass species, O and OH, approach a constant value at smaller inter-electrode distances as a result of their lower diffusion coefficients which mean that their surface losses become diffusion limited at shorter diffusion lengths.

For the higher H_2O content case (3 (b)), the trends in the density of the investigated species are different in comparison to the low H_2O content case. The normalised density of H still increases with increasing inter-electrode distance, however, the range of variation is less than in the low H_2O content case. This is a result of the higher densities of species with which H can react in the gas phase, which means that H atoms have a higher gas-phase consumption rate than in the low H_2O content case. This decreases the importance of surface consumption processes, and consequently the importance of the inter-electrode distance in defining the overall kinetics of H loss.

In the higher H_2O content case, the normalised OH density increases slightly with increasing inter-electrode distance, however, this increase is much less pronounced than in the case of the low H_2O content. Both H and OH are mainly produced via direct electron impact dissociation, the rate for which does not change significantly with increasing electrode distance. The observed changes can therefore be attributed to their consumption mechanisms.

The increase in the density of H is a result of its decreasing surface recombination rate. For the small electrode distance, the rate of recombination of H at the surface is higher than any gas-phase consumption rate contributing 88% to the total H consumption. For the largest electrode distance, the total rate of gas-phase consumption remains similar to the smallest electrode distance case while the rate of surface recombination decreases contributing only 2% to the total consumption. Overall, the increase in the H density is a result of the decrease in its total rate of consumption due to a decrease in its surface recombination rate.

Surface recombination plays a significantly smaller role in determining the OH density. At the smallest and largest investigated electrode distances, surface recombination contributes only 13% and less than 1% to the total consumption rate of OH, respectively. Therefore, in the absence of changes in its gas-phase consumption rate a small increase in OH density would be expected with increasing electrode distance. However, the gas-phase consumption also changes slightly due to the higher density of H. In particular, the rate for the reaction

$$OH + H + He \rightarrow H_2O + He \tag{18}$$

increases due to the increase in H density. Eq. 18 is the most significant consumption mechanism for OH in the gas-phase behind collisions between two OH radicals (eqs. (13) and (16)). The slightly decreased surface recombination and slightly increased gas-phase consumption due to the higher H density effectively cancel leading to an approximately constant OH density under variation of the electrode distance.

In contrast to the trends in the other investigated species densities, O decreases slightly with increasing inter-electrode distance at high H_2O content. This can be explained by the fact that surface processes do not play a significant role in the consumption of O at high H_2O content (less than 8% under all investigated conditions). However, the main consumption pathways for O are the reaction

$$O + H + He \rightarrow OH + He \tag{19}$$

which involves H, and destruction with OH according to eq. (14). Both of these species, particularly H, increase with higher inter-electrode distance. As a result, the density of O decreases slightly with increasing inter-electrode distance through increases in the rates of these consumption pathways.

4. Conclusion

The role of surface reaction probabilities and reactor geometry in determining the densities of reactive neutral species in a μAPPJ operated in a He-H_2O gas mixture were investigated using zero-dimensional plasma-chemical kinetics simulations. It was found that the choice of surface reaction probability, particularly γ_H, can lead to significant changes in the densities of reactive neutral species. This was found to be the case at both low and high feed gas H_2O mole fractions. In addition, the case of OH surface recombination was used to illustrate the importance of the surface reaction products.

Here, it was found that different product channels lead to distinctly different influences of OH surface recombination on gas phase species densities. This illustrates the potential complexity of these interactions and emphasises that a more sophisticated treatment of surface reactions, e.g. surface kinetics simulations, may be beneficial in simulating APP interactions with surfaces.

At low water admixtures the densities of O, H and OH in the plasma were found to depend on the reactor geometry. In particular, the density of H was found to vary by an order of magnitude depending on the reactor cross-section. Other species densities, such as O and OH, were also found to be affected by the reactor geometry, either directly because they react with surfaces (at low H_2O admixtures), or indirectly due to a change of reaction rates of plasma bulk reactions involving H (at high H_2O admixtures). Given these sensitivities, the choice of surface material as well as reactor dimensions could be tuned to tailor reactive species production in APPs, in particular, low-mass reactive species such as H, which do not readily react with the feedstock gases. From the perspective of technological or biomedical applications, this offers the opportunity to tailor the densities of reactive species propagating into the plasma effluent and therefore influence the plasma source efficacy in a given application. In addition, given that the choice of surface reaction probabilities can strongly influence predictions of reactive species densities in plasma simulations even at atmospheric pressure, care should be taken when using simulations to scale processes over large ranges of surface-to-volume ratio and surface materials.

5. Acknowledgements

This work was financially supported by the UK EPSRC (EP/K018388/1 & EP/H003797/2) and the York-Paris Low Temperature Plasma Collaborative Research Centre. The participation of MK was supported by the US Department of Energy (DE-SC0001319 and DE-SC0014132).

6. Bibliography

[1] M. G. Kong, G. Kroesen, G. Morfill, T. Nosenko, T. Shimizu, J. van Dijk, and J. L. Zimmermann. *New J. Phys.* **11** (2009) 115012.
[2] D. B. Graves. *J. Phys. D: Appl. Phys* **45** (2012) 263001.
[3] T. von Woedtke, S. Reuter, K. Masur, and K.-D. Weltmann. *Phys. Rep.* **530** (2013) 291–320.
[4] G. V. Lu, X .and Naidis, M. Laroussi, S. Reuter, D. B. Graves, and K. Ostrikov. *Phys. Rep.* **630** (2016) 1–84.
[5] J. Schlegel, J. Köritzer, and V. Boxhammer. *Clin. Plasma Med.* **1** (2013) 2–7.
[6] A. M. Hirst, F. M. Frame, N. J. Maitland, and D. O'Connell. *BioMed Res. Int.* **2014** (2014) 1–15.
[7] A. M. Hirst, F. M. Frame, M. Arya, N. J. Maitland, and D. O'Connell. *Tumor Biology* **37** (2016) 7021–7031.
[8] A. M. Hirst, M. S. Simms, V. M. Mann, N. J. Maitland, D. O'Connell, and F. M. Frame. *Br. J. Cancer* **112** (2015) 1536–1545.
[9] A. R. Gibson, H. O. McCarthy, A. A. Ali, D. O'Connell, and W. G. Graham. *Plasma Processes Polym.* **11** (2014) 1142–1149.

[10] R. S. Tipa and G. M. W. Kroesen. *IEEE Trans. Plasma Sci.* **39** (2011) 2978–2979.
[11] S. Bekeschus, A. Schmidt, K.-D. Weltmann, and T. von Woedtke. *Clin. Plasma Med.* **4** (2016) 19–28.
[12] M. Laroussi. *Plasma Process. Polym.* **2** (2005) 391–400.
[13] A. Privat-Maldonado, D. O'Connell, E. Welch, R. Vann, and M. W. van der Woude. *Sci. Rep.* **6** (2016) 35646.
[14] A. Hurlbatt, A. R. Gibson, S. Schröter, J. Bredin, A. P. S. Foote, P. Grondein, D. O'Connell, and T. Gans. *Plasma Process. Polym.* **14** (2016) 1600138.
[15] T. Murakami, K. Niemi, T. Gans, D. O'Connell, and W. G. Graham. *Plasma Sources Sci. Technol.* **22** (2013) 045010.
[16] T. Murakami, K. Niemi, T. Gans, D. O'Connell, and W. G. Graham. *Plasma Sources Sci. Technol.* **22** (2013) 015003.
[17] T. Murakami, K. Niemi, T. Gans, D. O'Connell, and W. G. Graham. *Plasma Sources Sci. Technol.* **23** (2014) 025005.
[18] W. Van Gaens and A. Bogaerts. *J. Phys. D: Appl. Phys.* **47** (2014) 079502.
[19] A. M. Lietz and M. J. Kushner. *J. Phys. D: Appl. Phys.* **49** (2016) 425204.
[20] D. X. Liu, P. Bruggeman, F. Iza, M. Z. Rong, and M. G. Kong. *Plasma Sources Sci. Technol.* **19** (2010) 025018.
[21] M. M. Turner. *Plasma Sources Sci. Technol.* **24** (2015) 035027.
[22] M. M. Turner. *Plasma Sources Sci. Technol.* **25** (2016) 015003.
[23] A. R. Gibson, M. Foucher, D. Marinov, P. Chabert, T. Gans, M. J. Kushner, and J.-P. Booth. *Plasma Phys. Control. Fusion* **59** (2017) 024004.
[24] D. A. Toneli, R. S. Pessoa, M. Roberto, and J. T. Gudmundsson. *J. Phys. D: Appl. Phys.* **48** (2015) 495203.
[25] A. Greb, A. R. Gibson, K. Niemi, D. O'Connell, and T. Gans. *Plasma Sources Sci. Technol.* **24** (2015) 044003.
[26] A. Greb, K. Niemi, D. O'Connell, and T. Gans. *Appl. Phys. Lett.* **103** (2013) 244101.
[27] S. Jacq, C. Cardinaud, L. Le Brizoual, and A. Granier. *Plasma Sources Sci. Technol.* **22** (2013) 055004.
[28] C. S. Moon, K. Takeda, S. Takashima, M. Sekine, Y. Setsuhara, M. Shiratani, and M. Hori. *J. Appl. Phys.* **107** (2010) 103310.
[29] O. Guaitella, M. Hübner, S. Welzel, D. Marinov, J. Röpcke, and A. Rousseau. *Plasma Sources Sci. Technol.* **19** (2010) 045026.
[30] T. Tsutsumi, A. Greb, A. R. Gibson, M. Hori, D. O'Connell, and T. Gans. *J. Appl. Phys.* **121** (2017) 143301.
[31] J. Guha, R. Khare, . Stafford, V. M. Donnelly, S. Sirard, and E. A. Hudson. *J. Appl. Phys.* **105** (2009) 113309.
[32] S. Gomez, P. G. Steen, and W. G. Graham. *Appl. Phys. Lett.* **81** (2002) 19–21.
[33] D Marinov, O Guaitella, J P Booth, and A Rousseau. *J. Phys. D: Appl. Phys.* **46** (2012) 032001.
[34] M. Sode, T. Schwarz-Selinger, W. Jacob, and H. Kersten. *J. Appl. Phys.* **116** (2014) 013302.
[35] V. Guerra. *IEEE Trans. Plasma Sci.* **35** (2007) 1397–1412.
[36] Y. C. Kim and M. Boudart. *Langmuir* **7** (1991) 2999–3005.
[37] G. Oinuma, Y. Inanaga, Y. Tanimura, M. Kuzumoto, Y. Tabata, and K. Watanabe. *J. Phys. D: Appl. Phys.* **43** (2010) 255202.
[38] C. M. Samuell and C. S. Corr. *J. Nucl. Mater.* **451** (2014) 211–215.
[39] G. Cunge, O. Joubert, and N. Sadeghi. *J. Appl. Phys.* **94** (2003) 6285–6290.
[40] A. Agarwal and M. J. Kushner. *J. Vac. Sci. Technol. A* **26** (2008) 498–512.
[41] R. Ono. *J. Phys. D: Appl. Phys.* **49** (2016) 083001.
[42] J. Benedikt, D. Schröder, S. Schneider, G. Willems, A. Pajdarová, J. Vlček, and V. Schulz-von der Gathen. *Plasma Sources Sci. Technol.* **25** (2016) 045013.
[43] K. Ding and M. A. Lieberman. *J. Phys. D: Appl. Phys.* **48** (2014) 035401.

[44] P. Bruggeman, G. Cunge, and N. Sadeghi. *Plasma Sources Sci. Technol.* **21** (2012) 035019.
[45] Y. Gorbanev, D. O'Connell, and V. Chechik. *Chem. Eur. J.* **22** (2016) 3496–3505.
[46] A. L. Sumner, E. J. Menke, Y. Dubowski, J. T. Newberg, R. M. Penner, J. C. Hemminger, L. M. Wingen, T. Brauers, and B. J. Finlayson-Pitts. *Phys. Chem. Chem. Phys.* **6** (2004) 604–613.
[47] A. H. Markosyan, A. Luque, F. J. Gordillo-Vázquez, and U. Ebert. *Comput. Phys. Commun.* **185** (2014) 2697–2702.
[48] J. Golda, J. Held, B. Redeker, M. Konkowski, P. Beijer, A. Sobota, G. Kroesen, N. St. J. Braithwaite, S. Reuter, M. M. Turner, T. Gans, D. O'Connell, and V. Schulz-von der Gathen. *J. Phys. D: Appl. Phys.* **49** (2016) 084003.
[49] J. Winter, K. Wende, K. Masur, S. Iseni, M. Dünnbier, U. Hammer, H. Tresp, K.-D. Weltmann, and S. Reuter. *J. Phys. D: Appl. Phys.* **46** (2013) 295401.
[50] K. Niemi, D. O'Connell, N. de Oliveira, D. Joyeux, L. Nahon, J. P. Booth, and T. Gans. *Appl. Phys. Lett.* **103** (2013) 034102.
[51] D. W. Liu, F. Iza, and M. G. Kong. *Appl. Phys. Lett.* **95** (2009) 031501.
[52] B. Niermann, T. Hemke, N. Y. Babaeva, M. Böke, M. J. Kushner, T. Mussenbrock, and J. Winter. *J. Phys. D: Appl. Phys.* **44** (2011) 485204.
[53] S. Schröter et al *"Absolute densities of atomic oxygen and hydroxyl radicals in an atmospheric pressure plasma containing humidity: UV and synchrotron VUV absorption spectroscopy and numerical simulations"* in preparation.
[54] G. V. Naidis. *Plasma Sources Sci. Technol.* **22** (2013) 035015.
[55] A. D. Tserepi and T. A. Miller. *J. Appl. Phys.* **75** (1994) 7231–7236.
[56] M. Suh, P. S. Bagus, S. Pak, M. P. Rosynek, and J. H. Lunsford. *J.Phys. Chem. B* **104** (2000) 2736–2742.